

Fractal-Based Point Processes

2005

Steven Bradley Lowen

*Harvard Medical School
McLean Hospital*

Malvin Carl Teich

*Boston University
Columbia University*

WILEY

5

Fractal and Fractal-Rate Point Processes



Jean-Baptiste Joseph Fourier (1768–1830) demonstrated that a time function could be constructed from a superposition of harmonic functions of different frequencies; the “Fourier transform” forms the basis of spectral analysis.



The Hungarian mathematician **Alfréd Haar (1885–1933)**, in his doctoral dissertation under David Hilbert, introduced a collection of simple orthogonal functions; these “Haar wavelets” initiated the field of time–scale analysis.

5.1	Measures of Fractal Behavior in Point Processes	103
5.1.1	Spectrum	103
5.1.2	Normalized Haar-wavelet variance	103
5.1.3	Normalized variance	105
5.1.4	Coincidence rate	105
5.1.5	Count autocorrelation	106
5.1.6	Scaling cutoffs and fractal-exponent estimates	107
5.2	Ranges of Power-Law Exponents	107
5.2.1	Negative values of α	107
5.2.2	Observed values of α	109
5.2.3	Limited range of the normalized variance exponent	109
5.2.4	Range of the normalized Haar-wavelet-variance exponent	111
5.2.5	Range of the normalized general-wavelet-variance exponent	113
5.3	Relationships among Measures	114
5.4	Examples of Fractal Behavior in Point Processes	115
5.4.1	$1/f$ noise	115
5.4.2	Normalized rate spectrum	116
5.4.3	Normalized Haar-wavelet variance	117
5.4.4	Normalized Daubechies-wavelet variance	120
5.5	Fractal-Based Point Processes	120
5.5.1	Fractal point processes	121
5.5.2	Fractal-rate point processes	123
5.5.3	Nonfractal point processes	124
5.5.4	Identification of fractal-based point processes	125
	Problems	126

As described in Chapter 2, fractals are objects whose measures exhibit scaling. We introduced point processes, along with their appurtenant measures, in Chapter 3, and set forth various examples in Chapter 4. With the fundamental properties of fractals and point processes in hand, we are now in a position to investigate the intersection of these two concepts.

In this chapter we consider various measures that are often used to establish the presence of fractal behavior in point processes. The spectrum and normalized Haar-wavelet variance turn out to be the measures of choice, as we will show. The mathematical techniques bequeathed to us by Fourier (1822) and Haar (1910) thus play especially important roles in the analysis of fractal-based point processes. By way of example, we examine a number of point processes in the biological and physical sciences using these preferred measures.

We then compare and contrast two general classes of point processes that exhibit fractal behavior: fractal point processes and fractal-rate point processes. We conclude by touching briefly on the process of deciding which point process might best describe an observed sequence of events.

5.1 MEASURES OF FRACTAL BEHAVIOR IN POINT PROCESSES

As shown in Sec. 2.2, a measure that exhibits scaling, when considered as a function of time or frequency, indicates power-law behavior. Power-law behavior, in turn, is often a harbinger of fractal behavior.

As demonstrated in Chapter 3, various relationships exist that link different measures of a point process. In principle, explicit knowledge of one such statistic leads directly to an exact form for another. Measures so linked might thus be expected to provide the same information, although in different form.¹ Power-law behavior is generally preserved among these measures since the relationships linking them generally involve integration, differentiation, Fourier transformation, and multiplication by integer powers of the argument of the measure.

5.1.1 Spectrum

In forging interrelationships among the various measures, we begin with the point-process spectrum $S_N(f)$ introduced in Sec. 3.5.2 (the reason that we begin with this measure will become apparent subsequently). Fractal behavior suggests itself when this quantity assumes the form

$$S_N(f) \approx (f/f_S)^{-\alpha} \quad (5.1)$$

over a range of frequencies (see Sec. 2.3), where f is taken to be positive.

In general, the power-law behavior of a statistic includes an exponent ($-\alpha$ in the case at hand) that characterizes the *relative strength* of the fluctuations at different frequencies (or times), as well as a multiplicative constant (f_S^α) that indicates the *absolute strength* of the fluctuations at all times (or frequencies).

For a point process with fractal characteristics, the value of $S_N(f)$ typically becomes larger as the frequency decreases, and an increasing share of fractal fluctuations is admitted. For spectral measures, power-law exponents therefore generally take on negative values, as shown in Eq. (5.1); we discuss this issue further in Sec. 5.2.1.

For similar reasons, we also observe negative values of the power-law exponents for measures that depend on a delay parameter, such as the count-based autocorrelation (which is a function of count index k) and the coincidence rate: correlation typically decreases with increasing delay.

5.1.2 Normalized Haar-wavelet variance

Given the spectrum $S_N(f)$, for all frequencies f , we obtain the normalized Haar-wavelet variance $A(T)$, for all counting times T , via Eq. (3.62). $A(T)$, which relies

¹ Actually, different measures are not entirely equivalent since they are subject to different inherent mathematical limitations, such as those discussed in Sec. 5.2. Moreover, real and finite data sets are affected by bias and variance that are not the same for all measures, as considered in detail in Chapter 12. These considerations lead us to conclude that the rate spectrum and normalized Haar-wavelet variance are generally the measures of choice.

on the simplest of wavelet basis functions (Haar, 1910), is constructed in accordance with the recipe provided in Sec. 3.4.3.

We now demonstrate that power-law behavior in $S_N(f)$ leads directly to power-law behavior in $A(T)$, with a related (but different) exponent and multiplicative constant:

$$A(T) \approx (T/T_A)^\alpha. \tag{5.2}$$

We begin with a spectrum $S_N(f)$ that varies in a power-law fashion, with exponent $-\alpha$ where $0 < \alpha < 1$:

$$S_N(f) = E^2[\mu] \delta(f) + E[\mu] [1 + (f/f_S)^{-\alpha}]. \tag{5.3}$$

Inserting Eq. (5.3) into Eq. (3.62) provides

$$\begin{aligned} A(T) &= \frac{4}{\pi^2 E[\mu] T} \int_{0+}^{\infty} S_N(f) \sin^4(\pi f T) f^{-2} df \\ &= \frac{4}{\pi^2 T} \int_0^{\infty} [1 + (f/f_S)^{-\alpha}] \sin^4(\pi f T) f^{-2} df \\ &= \frac{4}{\pi} \int_0^{\infty} [1 + (\pi f_S T/x)^\alpha] \sin^4(x) x^{-2} dx \\ &= 1 + (4/\pi)(\pi f_S T)^\alpha 2^\alpha (1 - 2^{\alpha-1}) \Gamma(1 - \alpha) \sin(\pi\alpha/2) / [\alpha(\alpha + 1)] \\ &= 1 + \frac{(2\pi f_S T)^\alpha (2 - 2^\alpha) 2 \sin(\pi\alpha/2) \Gamma(1 - \alpha)}{\alpha(\alpha + 1)\pi} \\ &\quad \times \frac{\sin(\pi\alpha)}{2 \sin(\pi\alpha/2) \cos(\pi\alpha/2)} \times \frac{\pi}{\Gamma(1 - \alpha) \Gamma(\alpha) \sin(\pi\alpha)} \end{aligned} \tag{5.4}$$

$$\begin{aligned} &= 1 + \frac{(2 - 2^\alpha) (2\pi f_S T)^\alpha}{\alpha(\alpha + 1) \Gamma(\alpha) \cos(\pi\alpha/2)} \\ &= 1 + \frac{(2 - 2^\alpha) (2\pi f_S)^\alpha}{\Gamma(\alpha + 2) \cos(\pi\alpha/2)} T^\alpha \end{aligned} \tag{5.5}$$

$$= 1 + (T/T_A)^\alpha, \tag{5.6}$$

which accords with Eq. (5.2) in the power-law regime. The notation $0+$ indicates that the integral excludes the delta function at $f = 0$, and the quantity $\Gamma(x)$ represents the (complete) Eulerian gamma function

$$\Gamma(x) \equiv \int_0^{\infty} t^{x-1} e^{-t} dt, \tag{5.7}$$

which we first met in Prob. 4.7. Both fractions following the multiplication signs in Eq. (5.4) are identically unity. For the first, this follows from the well-known double-angle trigonometric identity with an angle of $\pi\alpha/2$ whereas for the second it follows from a property of the Gamma function (Gradshteyn & Ryzhik, 1994, Eq. 8.334.3):

$$\Gamma(x) \Gamma(1 - x) \sin(\pi x) = \pi. \tag{5.8}$$

Comparing Eqs. (5.5) and (5.6) provides the constant T_A in terms of α and f_S :

$$\frac{1}{T_A^\alpha} = \frac{(2\pi f_S)^\alpha (2 - 2^\alpha)}{\Gamma(\alpha + 2) \cos(\pi\alpha/2)}. \quad (5.9)$$

Evidently, the fractal exponent $-\alpha$ in the spectrum, Eq. (5.3), transforms to the fractal exponent $+\alpha$ in the normalized Haar-wavelet variance, Eq. (5.6). These exponents are identical in magnitude but opposite in sign. Increasing the counting time typically increases the value of $A(T)$ for a point process with fractal characteristics so that power-law exponents for this measure generally take on positive values (see Sec. 5.2.1 for a further discussion of this issue). As the counting time for the Haar-wavelet variance increases, fractal fluctuations over larger and larger time scales are accessed by this measure.

Similar results obtain when generalizing the normalized Haar-wavelet variance $A(T)$ to an arbitrary wavelet basis.

5.1.3 Normalized variance

In a similar way, we obtain the normalized variance $F(T)$ from the spectrum $S_N(f)$ using Eq. (3.61). This quantity is constructed in accordance with the approach indicated in Sec. 3.4.2.

In this case we obtain

$$\begin{aligned} F(T) &= \frac{2}{\pi^2 \mathbb{E}[\mu] T} \int_{0+}^{\infty} S_N(f) \sin^2(\pi f T) f^{-2} df \\ &= \frac{2}{\pi^2 T} \int_0^{\infty} [1 + (f/f_S)^{-\alpha}] \sin^2(\pi f T) f^{-2} df \\ &= \frac{2}{\pi} \int_0^{\infty} [1 + (\pi f_S T/x)^\alpha] \sin^2(x) x^{-2} dx \\ &= 1 + \frac{(2\pi f_S)^\alpha}{\Gamma(\alpha + 2) \cos(\pi\alpha/2)} T^\alpha \end{aligned} \quad (5.10)$$

$$= 1 + (T/T_F)^\alpha, \quad (5.11)$$

where the cutoff time T_F is implicitly defined by Eqs. (5.10) and (5.11).

5.1.4 Coincidence rate

The coincidence rate $G(t)$ is related to the point-process spectrum $S_N(f)$ through a simple Fourier transform, as provided by Eq. (3.58).

In this case, as well, a power-law form for the coincidence rate emerges, along with its associated parameter t_G :

$$G(t) = \int_{-\infty}^{\infty} S_N(f) e^{i2\pi ft} df$$

$$\begin{aligned}
 &= \int_{-\infty}^{\infty} \{E^2[\mu] \delta(f) + E[\mu] + E[\mu] |f/f_S|^{-\alpha}\} e^{i2\pi ft} df \\
 &= E^2[\mu] + E[\mu] \delta(f) + 2E[\mu] \int_0^{\infty} (f/f_S)^{-\alpha} \cos(2\pi ft) df \\
 &= E[\mu] \delta(f) + E^2[\mu] + 2E[\mu] f_S^\alpha (2\pi|t|)^{\alpha-1} \int_0^{\infty} x^{-\alpha} \cos(x) dx \\
 &= E[\mu] \delta(f) + E^2[\mu] + 2E[\mu] f_S^\alpha (2\pi|t|)^{\alpha-1} \frac{\pi}{2\Gamma(\alpha) \cos(\pi\alpha/2)} \\
 &= E[\mu] \delta(f) + E^2[\mu] + E^2[\mu] \frac{(2\pi f_S)^\alpha}{2\Gamma(\alpha) \cos(\pi\alpha/2) E[\mu]} |t|^{\alpha-1} \\
 &= E[\mu] \delta(t) + E^2[\mu] [1 + (|t|/t_G)^{\alpha-1}]. \tag{5.12}
 \end{aligned}$$

5.1.5 Count autocorrelation

Finally, we determine the count autocorrelation by using Eqs. (5.12) and (3.54):

$$\begin{aligned}
 R_Z(k, T) &= \int_{-T}^T G(kT + t) (T - |t|) dt \\
 &= \int_{-T}^T \left\{ E^2[\mu] \left[1 + \left(\frac{kT + t}{t_G} \right)^{\alpha-1} \right] \right\} (T - |t|) dt, \quad k \neq 0 \\
 &= E^2[\mu] \int_{-T}^T (T - |t|) dt \\
 &\quad + E^2[\mu] \int_{kT-T}^{kT+T} (s/t_G)^{\alpha-1} (T - |s - kT|) dt \\
 &= E^2[\mu] T^2 + E^2[\mu] T^{1+\alpha} t_G^{1-\alpha} \int_{k-1}^{k+1} x^{\alpha-1} (1 - |x - k|) dx \\
 &= E^2[\mu] T^2 + E[\mu] T \frac{E[\mu] T^\alpha t_G^{1-\alpha}}{\alpha(1 + \alpha)} \\
 &\quad \times [(k + 1)^{\alpha+1} + (k - 1)^{\alpha+1} - 2k^{\alpha+1}]. \tag{5.13}
 \end{aligned}$$

The case $k = 0$ reduces to the mean square $E[Z_k^2(T)]$ so it need not be considered; this permits us to ignore the delta function at $t = 0$ in the coincidence rate. Hence, we assume $k > 0$ without loss of generality.

Using the binomial theorem, for large k Eq. (5.13) yields the simplified result

$$\begin{aligned}
 R_Z(k, T) &\approx E^2[\mu] T^2 + E[\mu] T \frac{E[\mu] T^\alpha t_G^{1-\alpha}}{\alpha(1 + \alpha)} \alpha(1 + \alpha) k^{\alpha-1} \\
 &= E^2[\mu] T^2 + (E[\mu] T) E[\mu] T^\alpha t_G^{1-\alpha} k^{\alpha-1} \\
 &= E^2[\mu] T^2 + (E[\mu] T) (T/T_R)^\alpha k^{\alpha-1}. \tag{5.14}
 \end{aligned}$$

5.1.6 Scaling cutoffs and fractal-exponent estimates

Some of the relationships obtained above remain intact in the absence of either a small- or large-size cutoff. Nevertheless, dispensing with either of these necessitates additional mathematical complexity for many of these equations, and renders others meaningless. Since all data derive from limited measurements, we adhere to the argument presented in Sec. 2.3.1 and focus on the situation where both cutoffs exist. This also has the merit of ensuring stationarity (Buckingham, 1983, Chapter 6).

From a theoretical standpoint, power-law behavior in one statistic generally implies the same in various other measures. Although any measure that takes a time or frequency argument can serve to characterize fractal behavior in a point process, in practice some statistics prove more useful than others. To distinguish among the various methods, we use subscripts to denote the values of α derived from particular functions, such as α_S and α_A for the values of α obtained from theoretical plots of the spectrum $S_N(f)$ and the normalized Haar-wavelet variance $A(T)$, respectively.

Furthermore, for a given finite-length data set, each measure returns an *estimate* of α , denoted $\hat{\alpha}$, and this stochastic value differs from the ideal value α in a random fashion. Combining notations, $\hat{\alpha}_A$ refers to a fractal-exponent estimate obtained from an estimated normalized Haar-wavelet variance function $\hat{A}(T)$, which, in turn, is calculated from a real, finite data set. In the context of characterizing fractal behavior in a point process, these estimates can suffer from a variety of shortcomings: excessive bias or variance in the measure itself, as mentioned in Chapter 3; a limited range of allowable power-law exponents, as discussed below; and excessive bias or variance in the resulting estimates of the power-law exponent and multiplicative constant, which we treat in detail in Chapter 12.

5.2 RANGES OF POWER-LAW EXPONENTS

5.2.1 Negative values of α

What ranges of fractal exponents are ordinarily observed in experiments? The measures set forth in Chapter 3 admit negative values of α , and the relationships considered in Sec. 5.1 essentially continue to hold, so this issue merits discussion.

Let us consider, for example, a spectrum that increases with frequency for $0 < f < f_S$:

$$S_N(f) = E^2[\mu] \delta(f) + E[\mu] \left[1 + \sqrt{f/f_S} \exp(-f/f_S) \right]. \quad (5.15)$$

The spectrum $S_N(f)$, as chosen, *increases* as \sqrt{f} for $0 < f \ll f_S$ so that in this frequency range, $S_N(f)$ exhibits $\alpha = -\frac{1}{2}$.

The corresponding coincidence rate, normalized variance, and normalized Haar-wavelet variance then become

$$G(t) = E[\mu] \delta(t) + E^2[\mu] + \sqrt{\pi/2} E[\mu] f_S (1 + x_n^2)^{-3/2} \times \left(\sqrt{\sqrt{x_n^2 + 1} + 1} - x_n \sqrt{\sqrt{x_n^2 + 1} - 1} \right) \tag{5.16}$$

$$F(T) = 1 + \frac{\sqrt{8}}{\sqrt{\pi} y_n} \left(\sqrt{\sqrt{y_n^2 + 1} + 1} - \sqrt{2} \right) \tag{5.17}$$

$$A(T) = 1 + \frac{\sqrt{2}}{\sqrt{\pi} y_n} \left(4\sqrt{\sqrt{y_n^2 + 1} + 1} - 3\sqrt{2} - \sqrt{\sqrt{4y_n^2 + 1} + 1} \right), \tag{5.18}$$

where $x_n = 2\pi f_S t$ is the normalized time for Eq. (5.16) while $y_n = 2\pi f_S T$ is the normalized time for Eqs. (5.17) and (5.18).

Over long time scales, corresponding to low frequencies $f \ll f_S$, these quantities approach

$$G(t) - E^2[\mu] \rightarrow - \left(E[\mu] / 4\pi \sqrt{f_S} \right) t^{-3/2} \tag{5.19}$$

$$F(T) - 1 \rightarrow \left(2/\pi \sqrt{f_S} \right) T^{-1/2} \tag{5.20}$$

$$A(T) - 1 \rightarrow \left(4 - \sqrt{2}/\pi \sqrt{f_S} \right) T^{-1/2}, \tag{5.21}$$

respectively. (For very large times, the outcomes are effectively indistinguishable from those for the homogeneous Poisson process.) Equations (5.19)–(5.21) are indeed in accord with the results provided in Sec. 5.1, provided that Eq. (5.12) is generalized to

$$G(t) = E[\mu] \delta(t) + E^2[\mu] [1 + \text{sgn}(\alpha) (t/t_G)^{\alpha-1}], \tag{5.22}$$

where $\text{sgn}(\alpha)$ denotes the sign of α .

However, as will become apparent in Sec. 5.4, values of α generally lie above zero and negative values almost never occur in practice. Fractal behavior typically exhibits increased fluctuations as the time grows larger and the frequency grows smaller, in contradiction to $\alpha < 0$. Moreover, the high-frequency cutoff would play a far more important role in this case. Since the spectrum would increase with frequency until reaching this cutoff, most of the power would lie just below the cutoff. In effect, therefore, such a signal would not differ appreciably from narrowband noise. As a result, this characteristic would dominate the behavior of the signal and would generally obscure any fractal properties that it might have. Revealing the scaling in this putative fractal signal would require integrating it a number of times until the resulting fractal exponent became positive. However, this would radically change the nature of the signal, thereby suggesting that the narrowband noise description of the signal would prove most useful.²

² A similar argument could be made for the low-frequency cutoff for fractal signals with positive fractal exponents α . However, a low-frequency cutoff does not affect the behavior of a signal within a window of duration significantly less than that cutoff. For negative fractal exponents, in contrast, the dominant high-frequency oscillation appears in windows of any duration greater than the inverse of the cutoff, particularly those with windows large enough to reveal the putative fractal behavior.

We conclude that negative values of α , although not prohibited, are generally not useful for fractal-based point processes. We therefore limit ourselves to values of α that are strictly positive.

5.2.2 Observed values of α

Experience shows that values of $\alpha > 2$, although not prohibited theoretically, rarely occur in practice. Furthermore, the process of estimating large values of α is problematical. The large rate of change attendant to such values, over even just a few orders of magnitude along the abscissa, leads to very large changes along the ordinate. As an example, consider a spectrum with $\alpha = 5$ and a spectrum of 1 kW/Hz at $f = 1$ Hz; at a frequency $f = 1$ kHz, the spectrum will have fallen to 1 pW/Hz, a factor of 10^{15} .

5.2.3 Limited range of the normalized variance exponent

Mathematical constraints limit the values that power-law exponents can attain for some statistics, affecting their usefulness in characterizing fractal behavior in point processes. We begin with the normalized variance $F(T)$, which has a power-law exponent that cannot exceed unity, as we now demonstrate.

In terms of the sequence of counts $\{Z_k(T)\}$ we have, by definition,

$$F(T) \equiv \frac{\text{Var}[Z(T)]}{\text{E}[Z(T)]}, \quad (5.23)$$

which reiterates Eq. (3.32). Consider now a larger counting window of duration nT , and express the new sequence of counts $\{Z_k(nT)\}$ in terms of the original sequence as

$$Z_k(nT) = \sum_{m=kn}^{kn+n-1} Z_m(T). \quad (5.24)$$

For the mean and variance of $Z_k(nT)$ we then have

$$\text{E}[Z_0(nT)] = \text{E}\left[\sum_{m=0}^{n-1} Z_m(T)\right] = \sum_{m=0}^{n-1} \text{E}[Z_m(T)] = n \text{E}[Z(T)] \quad (5.25)$$

$$\begin{aligned} \text{Var}[Z_0(nT)] &= \text{E}\left[\sum_{l=0}^{n-1} \left\{Z_l(T) - \text{E}[Z(T)]\right\} \sum_{m=0}^{n-1} \left\{Z_m(T) - \text{E}[Z(T)]\right\}\right] \\ &= \sum_{l=0}^{n-1} \sum_{m=0}^{n-1} \text{E}\left[\left\{Z_l(T) - \text{E}[Z(T)]\right\} \left\{Z_m(T) - \text{E}[Z(T)]\right\}\right] \\ &\leq \sum_{l=0}^{n-1} \sum_{m=0}^{n-1} \text{E}\left[\left\{Z_m(T) - \text{E}[Z(T)]\right\}^2\right] \\ &= n^2 \text{Var}[Z(T)], \end{aligned} \quad (5.26)$$

where we have set $k = 0$ without loss of generality for a stationary point process.

This results in an upper bound for the increase of the normalized variance:

$$F(nT) = \frac{\text{Var}[Z(nT)]}{\text{E}[Z(nT)]} \leq \frac{n^2 \text{Var}[Z(T)]}{n \text{E}[Z(T)]} = n \frac{\text{Var}[Z(T)]}{\text{E}[Z(T)]} = nF(T). \quad (5.27)$$

Thus, for an orderly, stationary point process, multiplying the counting time by an integer factor n permits the normalized variance to increase at most by that factor n . In particular, if the normalized variance follows the power-law form $F(T) = (T/T_F)^{\alpha_F}$, then the power-law exponent α_F cannot exceed unity.

Indeed, a number of point processes yield exponents that achieve the maximum value $\alpha_F = 1$. A nonfractal example is provided by an integrate-and-reset process with a rate that increases linearly between periodic resets. We illustrate this by choosing an integrate-and-reset point process with a rate given by

$$\mu(t) = \mu_0[1 + \cos(\omega_0 t + \theta)], \quad (5.28)$$

where ω_0 and μ_0 represent fixed, deterministic quantities with units of inverse time. The random variable θ , which is taken to be uniformly distributed between zero and 2π , renders the rate $\mu(t)$ and the resulting point process stationary.

For counting times T much larger than $1/\mu_0$, the number of counts will greatly exceed unity, justifying the approximations below. We then have

$$\begin{aligned} Z_0(T) &\approx \int_0^T \mu(t) dt = \int_0^T \mu_0[1 + \cos(\omega_0 t + \theta)] dt \\ &= \mu_0 T + \mu_0 \omega_0^{-1} [\sin(\omega_0 T + \theta) - \sin(\theta)] \\ &= \mu_0 T + 2\mu_0 \omega_0^{-1} \sin(\omega_0 T/2) \cos(\omega_0 T/2 + \theta) \end{aligned} \quad (5.29)$$

$$\text{E}[Z_0(T)] = \mu_0 T \quad (5.30)$$

$$\begin{aligned} \text{Var}[Z_0(T)] &\approx 4\mu_0^2 \omega_0^{-2} \sin^2(\omega_0 T/2) \text{E}[\cos^2(\omega_0 T/2 + \theta)] \\ &= 2\mu_0^2 \omega_0^{-2} \sin^2(\omega_0 T/2). \end{aligned} \quad (5.31)$$

If we further stipulate that the time scale of the sinusoid greatly exceeds that of the counting time, so that $1/\omega_0 \gg T$, then the rate approximates a linear function over the counting time T , and the results above simplify to

$$\begin{aligned} \text{Var}[Z_0(T)] &\approx 2\mu_0^2 \omega_0^{-2} [(\omega_0 T/2)^2 - (\omega_0 T/2)^4/3] \\ &= \mu_0^2 T^2/2 - \mu_0^2 \omega_0^2 T^4/24 \end{aligned}$$

$$F(T) \approx \mu_0 T/2 - \mu_0 \omega_0^2 T^3/24 \quad (5.32)$$

$$\approx \mu_0 T/2, \quad (5.33)$$

thereby demonstrating that this process does indeed achieve $\alpha_F = 1$. This result often emerges for nonfractal point processes with time-varying rates and when rate nonstationarities are present (see, for example Prucnal & Teich, 1979).

As with the normalized variance, values of α for the autocorrelation and coincidence rate necessarily lie below unity. Equation (3.51) establishes that for large

delay times, the coincidence rate approaches a constant value $E^2[\mu]$, while Eq. (5.12) exceeds this value by $E^2[\mu] (t/t_G)^{\alpha-1}$. In order that this quantity vanish for large t , so that the coincidence rate can achieve the limit provided in Eq. (3.51), it is required that $\alpha < 1$. Furthermore, application of Eq. (3.57) to a coincidence rate with $\alpha > 1$ would result in a spectrum that assumes negative values at large frequencies, an impossibility. This same argument applies to the autocorrelation $R_Z(k, T)$ (taken as a function of the delay index k), through Eq. (3.56).

The generalized dimensions of point processes encountered in the treatment provided here also lie below unity, because the dimension of any object may not exceed that of the space in which it is embedded. Lines have dimensions of unity, and we focus on point processes on a line.

For the point-process spectrum $S_N(f)$ [as well as for the rate spectrum $S_\lambda(f, T)$], in contrast, no such limit exists (however, see Prob. 5.12). Indeed, we chose the spectrum as a starting point in Sec. 5.1 precisely for this reason.

5.2.4 Range of the normalized Haar-wavelet-variance exponent

A more generous maximum exponent obtains for the normalized Haar-wavelet variance. We proceed in a similar fashion, beginning with the mean-square difference in the number of counts, and rearranging the sums to obtain

$$\begin{aligned}
 & E \left[\left\{ Z_0(nT) - Z_1(nT) \right\}^2 \right] \\
 &= E \left[\left\{ \sum_{m=0}^{n-1} Z_m(T) - \sum_{m=n}^{2n-1} Z_m(T) \right\}^2 \right] \\
 &= E \left[\left\{ \sum_{m=1}^n m \left[Z_{m-1}(T) - Z_m(T) \right] \right. \right. \\
 &\quad \left. \left. + \sum_{m=n+1}^{2n-1} (2n-m) \left[Z_{m-1}(T) - Z_m(T) \right] \right\}^2 \right] \\
 &\leq \left[\sum_{m=1}^n m + \sum_{m=n+1}^{2n-1} (2n-m) \right]^2 E \left[\left\{ Z_{m-1}(T) - Z_m(T) \right\}^2 \right] \\
 &= n^4 E \left[\left\{ Z_0(T) - Z_1(T) \right\}^2 \right]. \tag{5.34}
 \end{aligned}$$

Proceeding as previously, we obtain an upper bound for the increase of the normalized Haar-wavelet variance determined by

$$\begin{aligned}
 A(nT) &= E \left[\left\{ Z_0(nT) - Z_1(nT) \right\}^2 \right] / 2E[Z_0(nT)] \\
 &\leq n^4 E \left[\left\{ Z_0(T) - Z_1(T) \right\}^2 \right] / 2n E[Z_0(T)] \\
 &= n^3 A(T). \tag{5.35}
 \end{aligned}$$

This indicates a maximum factor of n^3 in the growth of the normalized Haar-wavelet variance as the counting time increases by n . The corresponding power-law exponent α_A therefore cannot exceed three, which is ample to accommodate all practical fractal-based point processes (see Sec. 5.2.2).

The same nonfractal integrate-and-reset process defined by Eq. (5.28), which achieved the maximum power-law exponent of unity for the normalized variance $F(T)$ for counting times T in the range $1/\mu_0 \ll T \ll 1/\omega_0$, also yields the maximum power-law exponent for the normalized Haar-wavelet variance $A(T)$. Combining Eqs. (3.41) and (5.32) provides

$$\begin{aligned} A(T) &= 2F(T) - F(2T) \\ &\approx \mu_0 T - \mu_0 \omega_0^2 T^3/12 - \mu_0 T + \mu_0 \omega_0^2 T^3/3 \\ &= \mu_0 \omega_0^2 T^3/4, \end{aligned} \quad (5.36)$$

indicating that this process again achieves the maximum permitted value, $\alpha_A = 3$, as do many nonstationary, nonfractal point processes.³

It is important to note that in deriving Eq. (5.36), we have made use of Eq. (5.32), rather than its approximation, Eq. (5.33). Using the latter yields incorrect results when linear terms dominate $F(T) - 1$. To illustrate this, suppose that over some range of counting times T , the normalized variance has a linear term that exceeds another contribution with a power-law form other than linear. To first order, we then have

$$\begin{aligned} F(T) &= 1 + c_1 T + c_2 T^\alpha \\ &\approx 1 + c_1 T. \end{aligned} \quad (5.37)$$

Based on this approximation, Eq. (3.41) yields

$$\begin{aligned} A(T) &= 2F(T) - F(2T) \\ &\approx 2 + 2c_1 T - (1 + 2c_1 T) \\ &= 1. \end{aligned} \quad (5.38)$$

However, the proper value of the normalized Haar-wavelet variance also contains a term that varies as T^α :

$$\begin{aligned} A(T) &= 2F(T) - F(2T) \\ &= 2 + 2c_1 T + 2c_2 T^\alpha - (1 + 2c_1 T + 2^\alpha c_2 T^\alpha) \\ &= 1 + (2 - 2^\alpha) c_2 T^\alpha. \end{aligned} \quad (5.39)$$

The disagreement between Eqs. (5.38) and (5.39) stems from improper use of asymptotic results in intermediate calculational steps. Equation (3.41) is correct and applies exactly in all cases. We conclude that when first-order approximations yield terms in $F(T)$ that are linear in T , we must retain the higher-order terms in calculating the normalized Haar-wavelet variance by means of Eq. (3.41).

³ Under some circumstances such nonstationarities can mask the presence of fractal behavior (see, for example, Turcott, Lowen, Li, Johnson, Tsuchitani & Teich, 1994).

5.2.5 Range of the normalized general-wavelet-variance exponent

Other wavelets offer even higher limits for their power-law exponents, as we now proceed to demonstrate (Teich et al., 1996; Heneghan, Lowen & Teich, 1996). We first recast Eq. (3.68) from a time domain integral into one in the frequency domain,

$$\begin{aligned} \text{Var}[C_{\psi,N}(a, b)] &= a \int_x G(ax) \int_y \psi(x+y) \psi(y) dy dx \\ &= a \int_x \int_f G(ax) |\varphi(f)|^2 e^{i2\pi fx} df dx \\ &= \int_f S_N(f/a) |\varphi(f)|^2 df, \end{aligned} \tag{5.40}$$

where

$$\varphi(f) = \int_x \psi(x) e^{-i2\pi fx} dx \tag{5.41}$$

represents the Fourier transform of the wavelet $\psi(x)$.

The behavior of $\varphi(f)$ near $f = 0$ determines the convergence properties of the integral in Eq. (5.40); this is related to n_v , the number of contiguous vanishing moments of the wavelet $\psi(t)$. We define n_v as the largest integer for which

$$\int \psi(t) t^k dt = 0 \tag{5.42}$$

for all k such that $0 \leq k \leq n_v$. The integral in Eq. (5.40) converges near the origin if the integrand increases more slowly than $1/f$ in that region. Given a spectrum that decays as $f^{-\alpha}$, this convergence requires that $2c > \alpha - 1$. A normalized wavelet variance constructed using a wavelet for which $|\varphi(f)| \sim f^c$ near $f \rightarrow 0$ will therefore faithfully reproduce power-law exponents α in the range $0 < \alpha < 2c + 1$.

As an example, we return to the Haar wavelet, which has

$$\begin{aligned} \varphi(f) &= 2ie^{i\pi f} \sin^2(\pi f/2) / f \\ |\varphi(f)| &= 2 \sin^2(\pi f/2) / f \sim f^1 \end{aligned} \tag{5.43}$$

near $f = 0$, so that $c = 1$, which yields a maximum power-law exponent of $2c+1 = 3$, as previously demonstrated in Eq. (5.35).

Wavelets other than the Haar have Fourier transforms that decay as f^c with $c > 1$, and therefore appear useful for the analysis of fractal processes with $\alpha > 3$. Such wavelets typically exhibit higher regularity and therefore have a higher number of vanishing moments. However, there is an important practical caveat regarding their use: they have larger support for a given scale and hence exhibit reduced scaling ranges for finite-length data sets (Heneghan et al., 1996), as is demonstrated in Fig. 5.3. Moreover, processes with $\alpha > 3$ do not often occur in practice so that the Haar wavelet usually suffices, as demonstrated in Sec. 5.4.4. Wavelets other than the Haar also enjoy the property of being insensitive to linear or higher-order polynomial trends, but in practice nonstationarities rarely follow a polynomial form. Finally, we note that wavelets with higher regularity yield wavelet transforms with less correlation among

the resulting wavelet coefficients, thereby improving the statistics of the resulting estimate (Tewfik & Kim, 1992). This also suggests the use of wavelets other than the Haar (Abry et al., 2003), but these wavelets turn out to yield *increased* variance in fractal-exponent estimates (Bardet, Lang, Oppenheim, Philippe, Stoev & Taquq, 2003), perhaps as a result of their larger support. We conclude that the Haar wavelet is generally the wavelet of choice for the analysis of point processes.

5.3 RELATIONSHIPS AMONG MEASURES

The relationships set forth in Sec. 5.1 all follow power-law forms. They are valid for $0 < \alpha < 1$ and display simple interrelations among their exponents over some range of the independent variables. Expressions over a range of times and frequencies are also available for all measures for $\alpha = 1$. For $\alpha > 1$, the limitations exposed in Sec. 5.2 tell us that the spectrum and normalized Haar-wavelet variance are the measures of choice; they offer extended validity over the range $0 < \alpha < 3$.

The relationships among the various measures over the full range $0 < \alpha < 3$ are summarized below:

- For $0 < \alpha < 1$:

$$\begin{aligned}
 S_N(f) &= E^2[\mu] \delta(f) + E[\mu] [1 + (f/f_S)^{-\alpha}] & \text{a)} \\
 F(T) &= 1 + (T/T_F)^\alpha & \text{b)} \\
 A(T) &= 1 + (T/T_A)^\alpha & \text{c)} \\
 R_Z(k, T) &= E^2[\mu] T^2 + (E[\mu] T) (T/T_R)^\alpha k^{\alpha-1} & \text{d)} \\
 G(t) &= E[\mu] \delta(t) + E^2[\mu] [1 + (|t|/t_G)^{\alpha-1}] & \text{e)}
 \end{aligned}
 \tag{5.44}$$

with

$$\begin{aligned}
 (2\pi f_S T_F)^\alpha &= \cos(\pi\alpha/2) \Gamma(\alpha + 2) & \text{a)} \\
 (T_F/T_A)^\alpha &= 2 - 2^\alpha & \text{b)} \\
 (T_F/T_R)^\alpha &= \frac{1}{2} \alpha(\alpha + 1) & \text{c)} \\
 E[\mu] t_G^{1-\alpha} T_R^\alpha &= 1 & \text{d)}
 \end{aligned}
 \tag{5.45}$$

where the limits $E[\mu] T \gg 1$ and $k \gg 1$ apply for Eq. (5.44d).

- For $\alpha = 1$:

$$\begin{aligned}
 S_N(f) &= E^2[\mu] \delta(f) + E[\mu] (1 + f_S/f) & \text{a)} \\
 F(T) &= 1 + 2f_S T \ln(B/T) & \text{b)} \\
 A(T) &= 1 + 4 \ln(2) f_S T & \text{c)} \\
 R_Z(k, T) &= E^2[\mu] T^2 + 2E[\mu] f_S \ln[B/(kT)] T^2 & \text{d)} \\
 G(t) &= E[\mu] \delta(t) + E^2[\mu] + 2f_S E[\mu] \ln(B/t) & \text{e)}
 \end{aligned}
 \tag{5.46}$$

where $S_N(f)$ is assumed to have a cutoff so that $F(T)$, $R_Z(k, t)$, and $G(t)$ exist.

- For $0 < \alpha < 3$:

$$\begin{aligned} S_N(f) &= E^2[\mu] \delta(f) + E[\mu] [1 + (f/f_S)^{-\alpha}] & \text{a)} \\ A(T) &= 1 + (T/T_A)^\alpha & \text{b)} \end{aligned} \quad (5.47)$$

with

$$(2\pi f_S T_A)^\alpha = \begin{cases} \cos(\pi\alpha/2) \Gamma(\alpha + 2)/(2 - 2^\alpha) & 0 < \alpha < 1 \\ \pi / [2 \ln(2)] & \alpha = 1 \\ [-\cos(\pi\alpha/2)] \Gamma(\alpha + 2)/(2^\alpha - 2) & 1 < \alpha < 3. \end{cases} \quad (5.48)$$

Equations (5.45) and (5.48) specify the relationships among the various **fractal onset times** and **fractal onset frequencies**. Earlier recitations of such relations appeared in Lowen & Teich (1993a, 1995), Thurner et al. (1997), and Ryu & Lowen (1998).

5.4 EXAMPLES OF FRACTAL BEHAVIOR IN POINT PROCESSES

Following a brief discussion of $1/f$ noise in the context of fractal-based continuous and point processes, we examine the estimated normalized spectrum and normalized Haar-wavelet variance for six representative biological point processes and one computer network traffic trace.

5.4.1 $1/f$ noise

Many forms of data, in many fields of endeavor, behave in accordance with the power-law spectrum specified in Eq. (5.1): $S(f) \approx (f/f_S)^{-\alpha}$. Signals with spectra of this form are typically referred to as **$1/f^\alpha$ noise** or **$1/f$ -type noise**. In the particular case when $\alpha = 1$, common appellations are **$1/f$ noise**, **flicker noise**, **excess noise**, and **pink noise**.⁴ Since no strict standard for this nomenclature exists, however, all of the foregoing descriptions are also used to describe $1/f^\alpha$ noise when α is in the rough vicinity of unity.

Fluctuations of this form are ubiquitous in the natural world. The earliest observation in the physical sciences appears to have been made by Johnson (1925), who discovered excess $1/f^\alpha$ noise in the course of his studies of low-frequency circuits. Such fluctuations are also widely present in electronic materials and devices, including

⁴ Spectra that are uniform in frequency are referred to as **white noise** in analogy with white light, which contains an equal weighting of all colors. If a spectrum obeys the form $S(f) \approx 1/f$, on the other hand, each octave is endowed with equal energy so that lower frequencies are weighed more heavily. By the same optical analogy, the red portion of the spectrum is then enhanced relative to the blue so that such spectra have come to be called **pink noise**. Spectra that follow the form $S(f) \approx 1/f^2$ should, by all rights, then be termed “red noise;” but are known instead as **brown noise** by virtue of their association with ordinary *Brownian* motion.

carbon resistors,⁵ thin-film resistors, semiconductors, metal films, electrolytes, superconductors, thermionic-emission devices, and junction devices (Bell, 1960, 1980; van der Ziel, 1988; Weissman, 1988; Buckingham, 1983; Kogan, 1996). In electronics, the range of frequencies over which such behavior is manifested can stretch over 12 orders of magnitude or more, and α typically lies between 0.8 and 1.4 (Buckingham, 1983, Chapter 6). The origins of this phenomenon remain obscure for many devices and systems. The underlying mechanism is often associated with fluctuations of the number, or the mobility, of the charge carriers, but other causes have been postulated. $1/f$ -type noise is thought by some to be a surface effect whereas others attribute it to bulk behavior. In the biological sciences, $1/f^\alpha$ noise appears to have been first observed by Verveen (1960) in his studies of membrane-voltage fluctuations.

Behavior of this kind is not restricted to simple materials, components, and devices. Complex systems also exhibit $1/f^\alpha$ noise; examples stretch from fluctuations of the flood level on the river Nile (Hurst, 1951), to voltage fluctuations in the human electroencephalogram (Musha, 1981), to measurements of cerebral blood flow (West, Zhang, Sanders, Miniyar, Zuckerman & Levine, 1999), to the formation of representations in a cognitive process (Gilden, 2001), to music deemed aesthetically pleasing to the listener (Gardner, 1978; Voss & Clarke, 1978; Voss, 1989; Hsü & Hsü, 1991). The ascendancy of fractal analysis in recent years has also drawn increased attention to $1/f$ noise (Mandelbrot, 1982; Montroll & Shlesinger, 1982; Shlesinger, 1987; Schroeder, 1990; West & Deering, 1995).

Our particular interest relates to the fluctuations observed in point processes rather than in continuous processes as highlighted above. Indeed, $1/f$ -type noise is ubiquitous in this domain as well.⁶ Early work along these lines was strongly influenced by Toshimitsu Musha and colleagues, who examined examples as diverse as vehicular traffic flow (Musha & Higuchi, 1976), spike-discharge intervals (Musha et al., 1983), human tapping intervals (Musha, Katsurai & Teramachi, 1985), and heartbeat period in humans (Kobayashi & Musha, 1982).

5.4.2 Normalized rate spectrum

In this section and the next, we examine second-order statistics for a collection of point processes. We plot the normalized estimated rate spectrum, $\hat{S}_\lambda(f, T)/\hat{E}[\lambda]$ vs. normalized frequency $f/\hat{E}[\lambda]$, in Fig. 5.1 for six biological point processes and one

⁵ Although ubiquitous, $1/f$ -type noise is not universal; it is not present, for example, in wire-wound resistors.

⁶ *Interval-based* spectra are often reported for point processes since calculating the spectrum of a discrete-time sequence is straightforward and the availability of the fast Fourier transform lowers the computational cost. Strictly speaking, the descriptor “ $1/f$ -type noise” should be used for such results, where f has units of cycles per number of intervals (see Sec. 3.3.3), but for simplicity we use the appellation “ $1/f$ -type noise” for both forms of the spectrum.

computer network traffic trace. To facilitate visual comparison, we have smoothed the spectra using a suitable windowing function.⁷

Figure 5.1 displays curves for the following point processes⁸: spontaneous vesicular exocytosis at a developing *Xenopus* neuromuscular junction (SYNAPSE) (Lowen et al., 1997b, Figs. 5 and 8, pp. 5670 and 5672, cell 950315e1); action-potential sequence recorded from a cat primary afferent auditory nerve fiber driven at its characteristic frequency of 10.2 kHz (COCHLEA) (Lowen & Teich, 1992a, the companion spontaneous recording is labeled “unit I”); action-potential sequences recorded from a cat on-center X-type retinal ganglion cell (RETINA) and its associated lateral geniculate nucleus cell (GENICULATE), in response to a 4.2-Hz drifting grating with 40% contrast and a mean luminance of 50 cd/m² (Lowen et al., 2001, Figs. 5D and 5E, p. 388, cells y31900ret and y31900lgn); action-potential sequence recorded from a cat layer-VI standard-complex striate cortex cell (CORTEX), in response to a weak steady background luminance ≈ 0.25 cd/m² (Teich et al., 1996, cell 3); 20-hour sequence of heartbeats recorded from a normal human subject (HEARTBEAT) (Turcott & Teich, 1996, data set 16273 from the MIT-BIH Normal Sinus Rhythm Database; available at <http://www.physionet.org/physiobank/database/nsrdb/>); and one million consecutive Ethernet-packet arrivals (COMPUTER) (Leland & Wilson, 1989, 1991, data set BC-pOct89 collected at the Bellcore Morristown Research and Engineering Facility in 1989; available at <http://ita.ee.lbl.gov/html/contrib/BC.html>).

All of the curves follow the general form of Eq. (5.1) over a range of normalized frequencies, $\hat{S}_\lambda(f, T)/\hat{E}[\lambda] \sim (f/f_S)^{-\alpha}$, suggesting the presence of fractal behavior. Similar results are obtained from the interval spectrum for these particular data sets (see Fig. 5.7 and Prob. 5.2).

5.4.3 Normalized Haar-wavelet variance

To complement the estimated spectral data displayed in Fig. 5.1, we present in Fig. 5.2 the estimated normalized Haar-wavelet variance $\hat{A}(T)$ vs. normalized counting time $T/\hat{E}[\tau]$ for the same six biological point processes and one computer network traffic

⁷ We smooth the measured rate and interval spectra by making use of the following procedure. We calculate the Fourier transform of the rate function (or interval sequence) and obtain its square magnitude. We then transform back into the time domain, which yields the autocorrelation. We multiply the autocorrelation by a triangular window with unity height at the origin, that decreases linearly to zero at one-eighth of the array size of the fast Fourier transform. Next we transform back to the frequency domain; this is the third Fourier transform involved in the smoothing procedure. The next step is to collect values into nonoverlapping blocks such that the largest frequency in a block, divided by the smallest, is as large as possible while lying below 1.02. Finally, all frequencies in each block are averaged and presented as a single frequency; the associated spectral values are similarly averaged. This procedure makes the graph appear progressively smoother as the frequency increases. The triangular windowing in the time domain is equivalent to subjecting the (noisy) periodogram to a moving-average $\text{sinc}^2(\cdot)$ filter in the frequency domain. This procedure reduces noise, but also reduces frequency resolution. Note that smoothing is generally eschewed before rigorous parameter estimation, as pointed out in Chapter 12.

⁸ These seven point processes are also examined in Figs. 5.2, 5.7–5.10, 11.2–11.4, 11.6–11.8, 11.10, 11.11, 11.13, and 11.14.

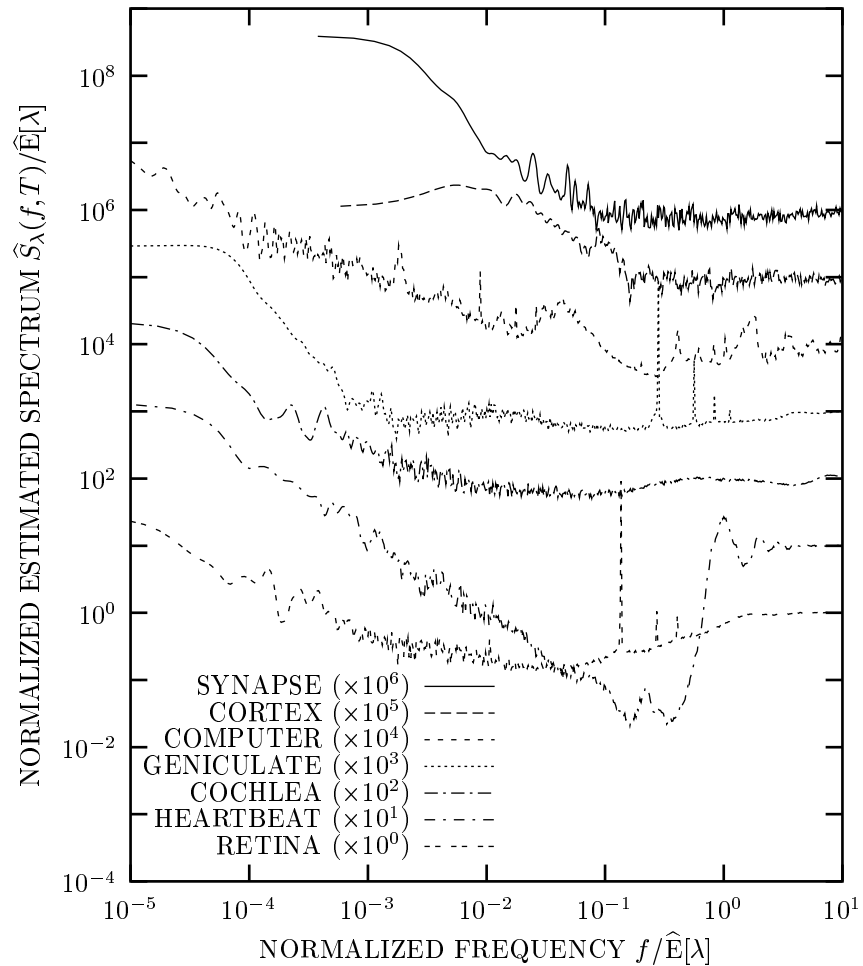


Fig. 5.1 Normalized estimated spectrum, $\hat{S}_\lambda(f, T)/\hat{E}[\lambda]$ vs. normalized frequency $f/\hat{E}[\lambda]$, for six biological point processes and one computer network traffic trace. The time T is chosen such that $1/\sqrt{2} < 30 T/E[\tau] < \sqrt{2}$, ensuring that the size of the Fourier-transform exceeds the number of intervals by a significant factor ($15\sqrt{2}$). Curves are displayed for the following point processes (see text for sources of data): vesicular exocytosis (SYNAPSE); action-potential sequence recorded from an auditory nerve fiber (COCHLEA); action-potential sequences recorded from a retinal ganglion cell (RETINA) as well as its associated lateral geniculate nucleus cell (GENICULATE); action-potential sequence recorded from a striate cortex cell (CORTEX); day-long sequence of normal human heartbeats (HEARTBEAT); and one million consecutive Ethernet-packet arrivals (COMPUTER). The curves decrease with frequency roughly as power laws, with seven negative estimated power-law exponents $-\hat{\alpha}_S$.

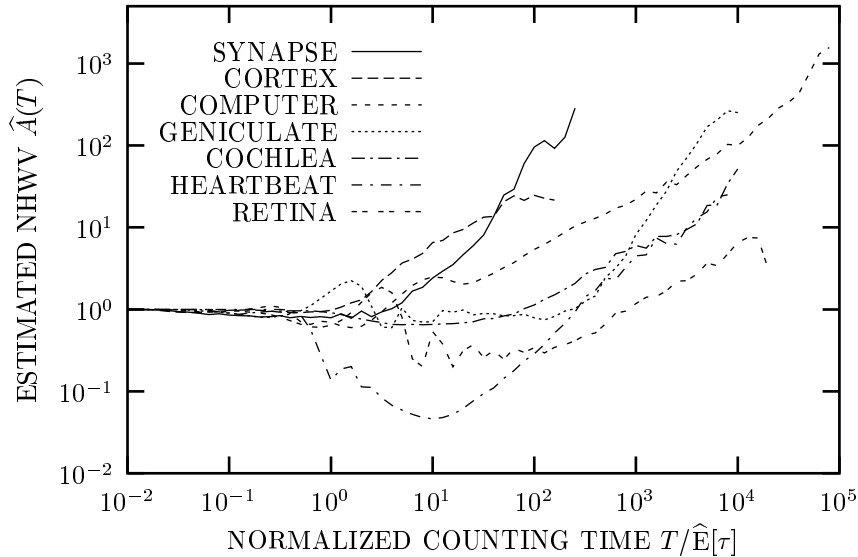


Fig. 5.2 Estimated normalized Haar-wavelet variance (NHV), $\hat{A}(T)$ vs. normalized counting time $T/\hat{E}[\tau]$, for the same seven point processes as displayed in Fig. 5.1. We present curves for the following point processes (see text for sources of data): vesicular exocytosis (SYNAPSE); action-potential sequence recorded from an auditory nerve fiber (COCHLEA); action-potential sequences recorded from a retinal ganglion cell (RETINA) as well as its associated lateral geniculate nucleus cell (GENICULATE); action-potential sequence recorded from a striate cortex cell (CORTEX); day-long sequence of normal human heartbeats (HEARTBEAT); and one million consecutive Ethernet-packet arrivals (COMPUTER). The curves increase roughly as straight lines, indicating approximate power-law dependence on the counting time, with seven positive estimated power-law exponents $\hat{\alpha}_A$.

trace. The calculations made use of counting times T that increased geometrically by factors of $10^{0.1}$, providing 10 counting times per decade.

These curves are the time-scale equivalents of $1/f^\alpha$ fluctuations. They follow the general form of Eq. (5.2) over a range of normalized counting times, $A(T) \approx (T/T_A)^\alpha$. The normalized interval wavelet variance for these data provide further evidence for power-law behavior (see Fig. 5.8 and Prob. 5.3). All of these results together lend credence to the notion that the data exhibit fractal behavior, as suggested by the results presented in Sec. 5.4.2.

In spite of its ubiquity, the fractal behavior evident in these point processes should not be ascribed to any single physical or biological mechanism. As demonstrated in the following chapters, behaviors in accordance with $1/f^\alpha$ and T^α are inherent in essentially all fractal-based point processes, under suitable conditions.

5.4.4 Normalized Daubechies-wavelet variance

Of all possible wavelets, the Haar has compact support and also has the best localization in time. This temporal precision, must, of course, be traded against scale resolution by virtue of the uncertainty principle.

Ingrid Daubechies (1988) developed a family of wavelets with compact support and differing abilities to localize signals in time and scale. The Haar forms the simplest and first member of this family. Daubechies wavelets are defined in terms of discrete-time filters with n coefficients, or “taps,” with n an even positive integer. Orthogonality requirements yield $n/2$ equations for these coefficients. To specify the other $n/2$ equations, and thus to determine the coefficients, Daubechies set the filter response to zero for polynomials of order less than $n/2$.

The Haar wavelet, which is equivalent to the Daubechies 2-tap wavelet, is therefore insensitive to constant values, whereas the Daubechies 20-tap wavelet, for example, is insensitive to polynomials up to and including order nine. Increasing the number of taps enhances the scale localization, but at the expense of a loss in time precision. This polynomial insensitivity is salutary inasmuch as it mitigates against some forms of nonstationarity that might be present in the point process although, as discussed in Sec. 5.2.5, nonstationarities do not always follow polynomial forms.

To illustrate the behavior of wavelets beyond the Haar, we plot the estimated normalized Daubechies-wavelet variance $\hat{A}_W(T) \equiv \widehat{\text{Var}}[C_{\psi,N}(T, \cdot)]/\widehat{\text{E}}[\lambda_k(T)]$ for a sequence of geniculate action potentials, as a function of the normalized counting time $T/\widehat{\text{E}}[\tau]$, in Fig. 5.3. In this case we calculate the wavelet variance using four different Daubechies wavelets: 2-tap, 8-tap, 14-tap, and 20-tap, as indicated in the figure. The four curves all begin at a normalized counting time of 0.1 by construction. For large counting times the curves all increase roughly as straight lines, yielding four exponents $\hat{\alpha}_W$, all of which are essentially the same. For this finite-length data set, the scaling region shrinks as the wavelet support increases with the number of taps, confirming the suggestion set forth in Sec. 5.2.5 that the Haar wavelet generally suffices for the analysis of fractal-based point processes.

5.5 FRACTAL-BASED POINT PROCESSES

The statistical measures described in Sec. 5.3, and examined in Sec. 5.4 for various experimental point processes, are second-order relationships. As such, they provide important, but limited, information about the underlying point process. We now proceed to further specify these underlying point processes.

In this section we compare and contrast two mutually exclusive classes of fractal-based point processes: fractal point processes and fractal-rate point processes. Both forms are found in the physical and biological sciences. Specific models that belong to these classes are examined in Chapters 6–10, where we study their full properties. We also devote a portion of this section to re-examining and confirming the nature of the nonfractal point processes introduced in Chapter 4, and we briefly consider the identification of fractal-based point processes.

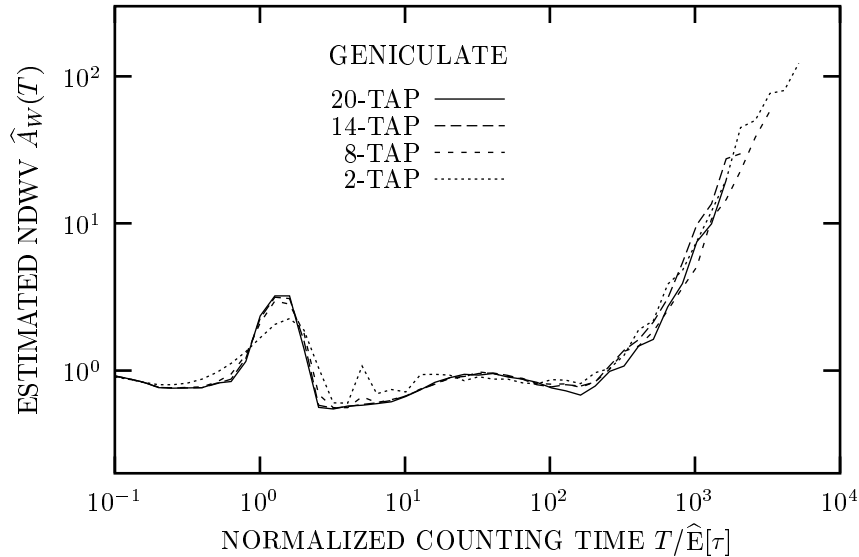


Fig. 5.3 Estimated normalized Daubechies-wavelet variances (NDWV), $\hat{A}_W(T)$ vs. normalized counting time $T/\hat{E}[\tau]$, for an action-potential sequence recorded from a cat on-center X-type lateral geniculate nucleus cell in response to a 4.2-Hz drifting grating with 40% contrast and a mean luminance of 50 cd/m² (Lowen et al., 2001, cell y31900lgn). Results are shown for four Daubechies wavelet bases: 2-tap (Haar), 8-tap, 14-tap, and 20-tap. The scaling region decreases as the wavelet support increases with the number of taps.

5.5.1 Fractal point processes

We define a **fractal point process** as one that has the following properties:

- $0 < \alpha < 1$
 1. Scaling behavior in the spectrum $S_N(f)$, coincidence rate $G(t)$, autocorrelation $R_Z(k, T)$, normalized variances $F(T)$ and $A(T)$, and interval probability density function $p_\tau(t)$.
 2. Simply related exponents, as in Eq. (5.44).
 3. Generalized dimensions D_q in the sense of Eq. (3.72), with $D_q = D = \alpha$ for all q .

Because all exponents and generalized dimensions coincide, the collection of measures specified above are characterized by a single value, α , that describes the scaling behavior. Since D_q cannot exceed unity for a collection of points on a line, and the upper bound of unity leads to a degenerate point process, we have $\alpha < 1$. In addition, as discussed in Sec. 5.2.1, we require $\alpha > 0$. Taken together, these two limits yield $0 < \alpha < 1$ for a fractal point process, as indicated above.

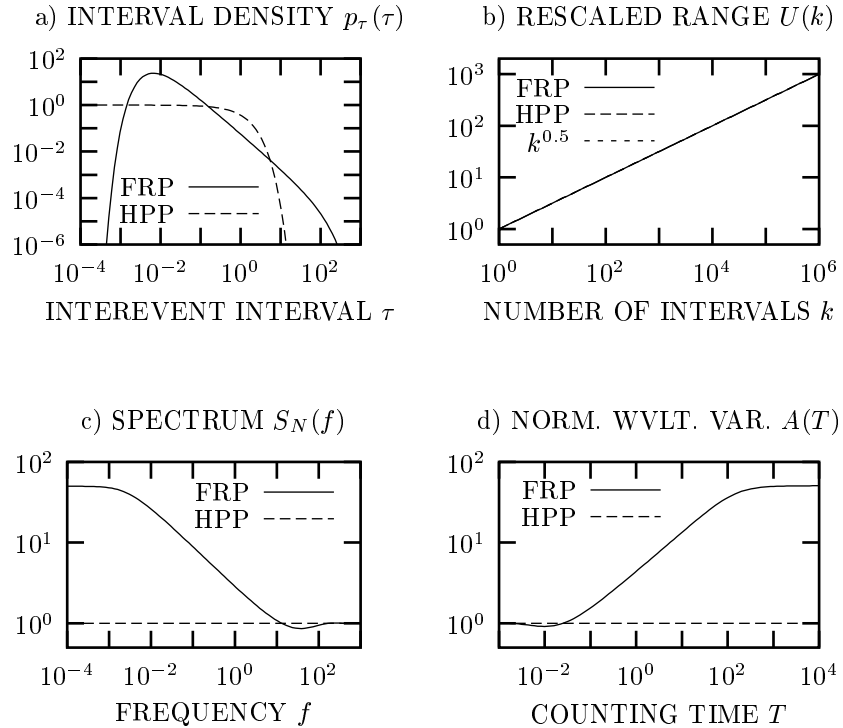


Fig. 5.4 Comparison of measures for a particular fractal point process, the fractal renewal process (FRP; see Chapter 7); and a point process that is devoid of fractal properties, the homogeneous Poisson process (HPP; see Sec. 4.1). We plot cartoons for four different probabilistic measures: (a) interevent-interval probability density, (b) rescaled range, (c) point-process spectrum, and (d) normalized Haar-wavelet variance. The rescaled-range measure cannot differentiate between these two processes since both belong to the family of renewal point processes. However, the other three measures exhibit nontrivial power-law variations for the fractal point process, but not for the nonfractal process.

The **intermittency**, which quantifies the unevenness of a point process, is defined as $1 - D_2$; it assumes a value of zero for a perfectly periodic point process, in which all intervals are identical, and approaches unity for a highly clustered process (Bickel, 1999). Since $D_2 = \alpha$ for fractal point processes, the intermittency is $1 - \alpha$.

In Fig. 5.4, we display the statistics of the nonfractal homogeneous Poisson process described in Sec. 4.1, together with a particular fractal point process, the **fractal renewal process** discussed in Chapter 7. This process exhibits scaling behaviors in all of the measures listed above and indeed has $D_q = \alpha$ for all q . In particular, realizations of this process are fractal.

Several of the interval-based measures described in Sec. 3.3 do *not* indicate fractal behavior for this process, which is, by definition, fractal. This is because the

process is renewal (see Sec. 4.2) so that the intervals between adjacent events $\{\tau_n\}$ are independent and identically distributed. Thus, results that are indistinguishable from those of other, nonfractal renewal point processes (see Sec. 5.5.3) emerge for the interval-based autocorrelation $R_\tau(k)$, interval spectrum $S_\tau(f)$, interval wavelet variance $\text{Var}[W_{\psi,\tau}(k,l)]$, rescaled range $U(k)$, and detrended fluctuation $Y(k)$. As a consequence, these interval-based measures are not suitable for determining the presence or absence of fractal behavior in general fractal-based point processes, which comprise both fractal and fractal-rate point processes (see Sec. 12.3.1). We therefore use interval-based measures judiciously in the remainder of this book.

Fractal point processes comprise hierarchies of clusters. This can arise if the interevent intervals are power-law distributed or if they exhibit long-range positive correlations. An example of a fractal point process that is distinct from the fractal renewal process arises from an infinitely divisible cascade (Castaing, 1996).

Consider a multiplicative-rate point process (Schmitt, Vannitsem & Barbosa, 1998) that begins with a constant rate over a fixed interval. Divide the interval into m subintervals, and multiply each by a random number, $W_{1,k}$, $1 \leq k \leq m$. Apply the same procedure to each subinterval, and then, in turn, to each sub-subinterval, *ad infinitum*. The weighting factors $W_{l,k}$, $1 \leq k \leq m^l$, are independent, identically distributed, unit-mean, nonnegative random variables.

A particular implementation of this process sets conditions on the weights applied to each new interval by the next stage of multiplication (Riedi, 2003). Let $Q_{l,nm} \equiv \frac{1}{m} \sum_{k=mn+1}^{m(n+1)} W_{l,k}$ denote an average, where n is any integer between 0 and m^{l-1} , inclusive. Two conditions on $Q_{l,nm}$ can be imposed for all values of l and n specified above: either $Q_{l,nm} = 1$ or $E[Q_{l,nm}] = 1$. When employed as a rate for a doubly stochastic or integrate-and-reset process, as described in Secs. 4.3 and 4.4, respectively, it turns out that the resultant point process belongs to the family of fractal point processes (Bickel, 1999).

One formalism for generating a *multifractal* process emerges by changing the time axis of a monofractal process to another process with multifractal characteristics. For example, $B_H(t) \equiv B_H[M(t)]$, where $B_H(t)$ represents fractional Brownian motion (see Chapter 6) and $M(t)$ is a nondecreasing, multifractal process (Mandelbrot, 1997, 1999). A number of variations on these processes exist (Peltier & Lévy Véhel, 1995; Benassi, Jaffard & Roux, 1997; Ayache & Lévy Véhel, 1999).

5.5.2 Fractal-rate point processes

Many point processes do not have fractional values of D_q , but nevertheless exhibit scaling behavior in other measures. Realizations of such processes are not fractals. Instead, the scaling behavior implies fractal characteristics of the *rates* associated with these point processes: the rate estimated from a realization of the process $[\lambda_k(T)]$ and the probabilistic rate that provides a mathematical description of the process $[\mu(t)]$ (Kumar & Johnson, 1993). Since the fractal behavior inheres to the rate rather than to the point process itself, we denote these as fractal-rate point processes.

We thus define a **fractal-rate point process** as one that is *not* a fractal point process and has the following properties:

- For $0 < \alpha < 1$:
 1. Scaling behavior in the spectrum $S_N(f)$, coincidence rate $G(t)$, autocorrelation $R_Z(k, T)$, and normalized variances $F(T)$ and $A(T)$.
 2. Simply related exponents, as in Eq. (5.44).
- For $1 \leq \alpha < 3$:
 1. Scaling behavior in the spectrum $S_N(f)$ and normalized Haar-wavelet variance $A(T)$.
 2. Exponents of these two measures sum to zero,

$$\alpha_A + (-\alpha_S) = 0. \quad (5.49)$$

Fractal-rate point processes can, in principle, exhibit any positive value of α ; values in excess of two rarely occur in practice, however, as discussed in Sec. 5.2.2. All of the fractal-based point processes considered in this book belong to the fractal-rate family, with the exception of the fractal renewal point process and the infinitely divisible cascade discussed in Sec. 5.5.1.

In Fig. 5.5, we display the statistics of the nonfractal **homogeneous Poisson process** described in Sec. 4.1, together with a particular fractal-rate point process, the **fractal-Gaussian-process-driven Poisson process**. This is a doubly stochastic Poisson process driven by a fractal Gaussian process; we consider it in detail in Secs. 6.3.3, 8.4, and 10.6.1, as well as in Chapter 12. For this point process, the spectrum, coincidence rate, count autocorrelation, and normalized count variances all scale with their respective arguments. However, it is a fractal-rate point process and not a fractal point process since the interevent-interval density is exponentially (rather than power-law) distributed and since D_q assumes integer values for all q (see Prob. 5.5).

Examination of Figs. 5.4 and 5.5 shows that the two interval-based measures fail to reliably reveal fractal-based behavior in a point process, whereas the other two measures do. We address this issue in greater detail in Sec. 12.3.1.

5.5.3 Nonfractal point processes

In light of the foregoing definitions, the processes described in Chapter 4 are certainly “nonfractal.”

Consider first the homogeneous Poisson process, described in Sec. 4.1. Examination of the measures set forth in that section reveals that none exhibit power-law behavior or scaling, except for trivial, integer powers in the count-based autocorrelation. Thus, the homogeneous Poisson process belongs to the class of nonfractal processes.

Renewal point processes and doubly stochastic Poisson processes both have fractal-based versions, as we have seen and shall see again in subsequent chapters. In general,

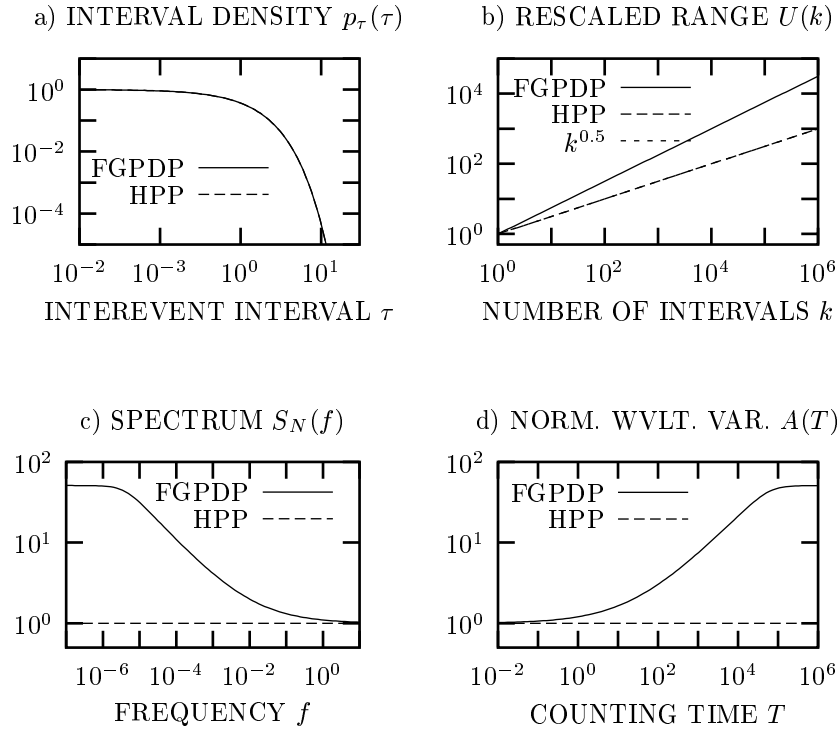


Fig. 5.5 Comparison of measures for a particular fractal-rate point process, the fractal-Gaussian-process-driven Poisson process with $\alpha = \frac{1}{2}$ (FGPDP; see Chapters 6, 8, 10, and 12); and a point process that is devoid of fractal properties, the homogeneous Poisson process (HPP; see Sec. 4.1). We plot cartoons for the same four probabilistic measures shown in Fig. 5.4: (a) interevent-interval probability density, (b) rescaled range, (c) point-process spectrum, and (d) normalized Haar-wavelet variance. For small values of the rate coefficient of variation, the interevent-interval probability density does not differentiate between these two processes [see Eq. (4.33)], although the intervals have different ordering in the two cases. However, the other three measures exhibit nontrivial power-law variations for the fractal-rate point process, but not for the nonfractal process.

however, these two classes of processes do not exhibit fractal characteristics, as is evident in Secs. 4.2 and 4.3, which leads us to term the general versions thereof as “nonfractal.”

5.5.4 Identification of fractal-based point processes

A worthy goal of point-process analysis is the association of a particular point-process model with an observed point process. The ability to exclude competing models serves

to narrow the range of possible mechanisms that could plausibly give rise to the data, thereby opening a window on the underlying science.

Because of the sparseness of point-process data, this is generally not an easy task. Consider the simple example of a fractal-rate point process. Rate fluctuations at frequencies significantly higher than the mean rate of the generated point events are essentially not transferred to the point process. Hence, details that could elucidate the nature of the rate process are lost. Moreover, no single statistic is sufficient to identify or characterize a fractal-based point process. Nevertheless, under certain circumstances, progress toward the identification of a fractal-based point process can be achieved by using a number of statistics in concert (see, for example, Rangarajan & Ding, 2000; Greis & Greenside, 1991).

We present a simple example that relies on the distinctions between fractal and fractal-rate point processes drawn earlier in this Section. If the estimated spectrum (Sec. 3.5.2) of the point process under study, $\hat{S}_N(f)$, strongly indicates the presence of fractal behavior, while the estimated interval spectrum (Sec. 3.3.3) of the process, $\hat{S}_\tau(f)$, does not, then the point process in question may well belong to the fractal-renewal-process family. Further confirmation of such a hypothesis is provided by shuffling the intervals (see Sec. 11.5) and then recomputing the spectra. A renewal point process, whether fractal or not, is invariant to such shuffling since its interevent intervals are independent and identically distributed. A more direct approach to distinguishing between fractal and fractal-rate point processes relies on the generalized dimension D_q (see Prob. 5.5).

Further discussion related to the identification of point processes is deferred to Chapters 11 and 13, following the introduction of various fractal-based point-process models in Chapters 6–10.

Problems

5.1 *Rate-spectrum and wavelet-variance scaling-exponent estimates for experimental point processes* Consider the spectrum and normalized Haar-wavelet variance provided in Figs. 5.1 and 5.2.

5.1.1. Obtain estimates for the scaling exponents $\hat{\alpha}_S$ and $\hat{\alpha}_A$ for the COMPUTER and GENICULATE data. Show that $\hat{\alpha}_A + (-\hat{\alpha}_S) \approx 0$, in accordance with Eq. (5.49). Explain why the two exponents do not sum precisely to zero.

5.1.2. A plot of the normalized variance $\hat{F}(T)$ vs. normalized counting time $T/\hat{E}[\tau]$ for the COMPUTER and GENICULATE data appears in Fig. 5.6. The counting times T increase geometrically by factors of $10^{0.1}$, providing 10 counting times per decade. We also show theoretical curves that fit the data; these exhibit exponents $\hat{\alpha}_F = 0.8$ and 1.0 , respectively. Compare these values with $\hat{\alpha}_S$ and $\hat{\alpha}_A$ for the two data sets and comment on any discrepancy.

5.2 *Interval-spectrum scaling-exponent estimates for experimental point processes*

Plots of the interval spectrum, $\hat{S}_\tau(f)/\widehat{\text{Var}}[\tau]$ vs. interval frequency f , are displayed in Fig. 5.7 for seven experimental point processes.

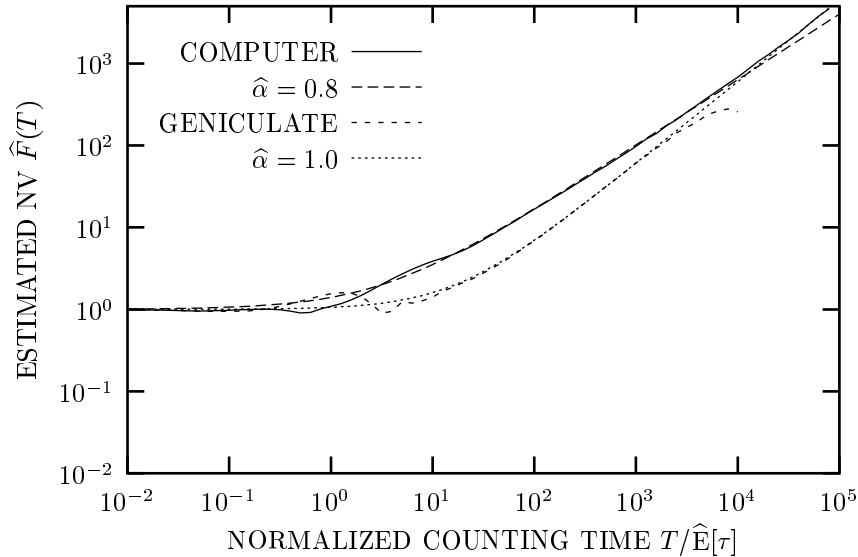


Fig. 5.6 Estimated normalized variance $\hat{F}(T)$ vs. normalized counting time $T/\hat{E}[\tau]$ for the COMPUTER and GENICULATE data displayed in Figs. 5.1 and 5.2. Also shown are the best fitting theoretical curves. For sufficiently large counting times, these curves increase roughly as straight lines, indicating an approximate power-law dependence on the counting time, with estimated power-law exponents $\hat{\alpha}_F$.

5.2.1. Using the graphs provided in Figs. 5.1 and 5.7, determine whether $\hat{\alpha}_S$ and $\hat{\alpha}_{S\tau}$ are less than, or greater than, unity for all data sets. In making these estimates, restrict yourself to the decreasing straight-line portions of the curves.

5.2.2. Using only the data displayed in Fig. 5.1, determine which of the point processes are likely represented by: (i) a fractal-based point process, (ii) a fractal point process, (iii) a fractal renewal process, (iv) a fractal-rate point process.

5.2.3. Now, consider the curves displayed in Fig. 5.7 in conjunction with those shown in Fig. 5.1. Using the information provided by both measures, which of the point processes are likely represented by: (i) a fractal-based point process, (ii) a fractal point process, (iii) a fractal renewal process, (iv) a fractal-rate point process?

5.2.4. Can $S_\tau(f)$ provide a good estimate of the fractal exponent?

5.2.5. Why is $f = \frac{1}{2}$ the maximum interval frequency plotted for $S_\tau(f)$?

5.3 *Interval-wavelet-variance scaling-exponent estimates for experimental point processes* Figure 5.8 displays the estimated normalized interval wavelet variance, $\hat{A}_\tau(k) = \widehat{\text{Var}}[W_{\psi,\tau}(k,l)]/\widehat{\text{Var}}[\tau]$ vs. number of intervals k [see Eq. (12.13)], for seven experimental point processes, calculated using the Haar wavelet.

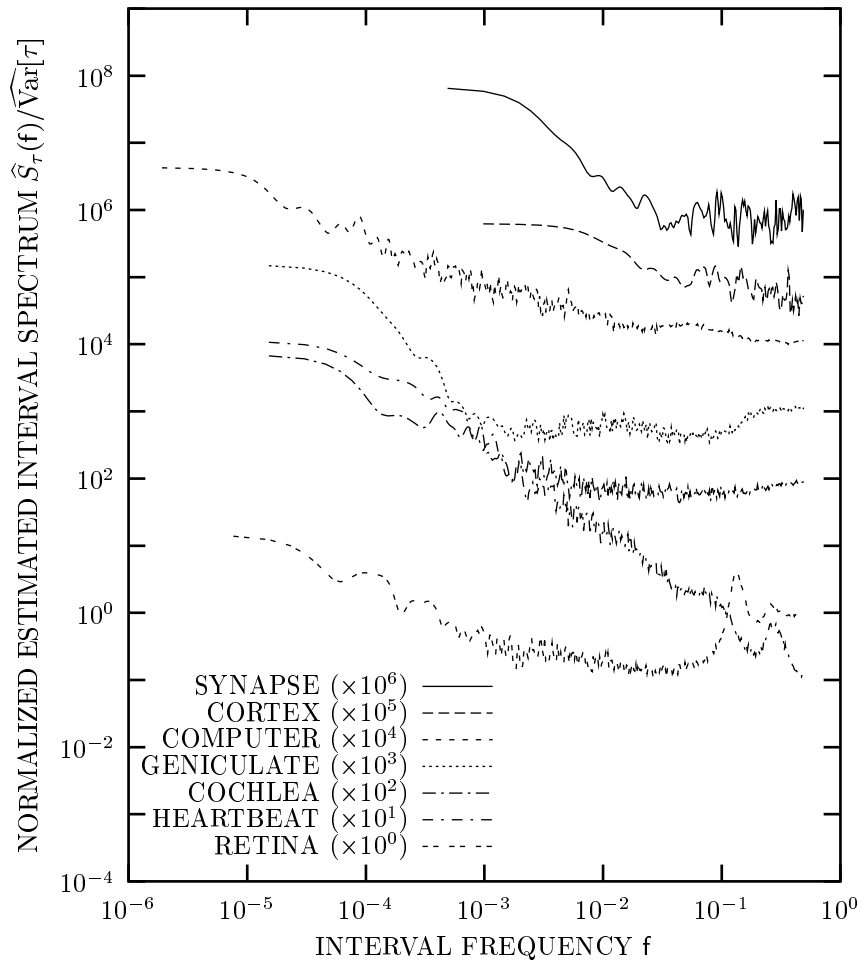


Fig. 5.7 Normalized estimated interval spectrum, $\hat{S}_\tau(f)/\widehat{\text{Var}}[\tau]$ vs. interval frequency f , for the same seven point processes as displayed in Fig. 5.1. We have smoothed the spectra to facilitate comparison (see Footnote 7 on p. 117). For sufficiently low interval frequencies, these curves decrease roughly as straight lines. This indicates an approximate power-law dependence on the interval frequency, with seven negative estimated power-law exponents $-\hat{\alpha}_{S\tau}$.

5.3.1. Using the graphs provided in Figs. 5.2 and 5.8, determine whether $\hat{\alpha}_A$ and $\hat{\alpha}_{A\tau}$ are less than, or greater than, unity for all data sets. Restrict yourself to the increasing straight-line portions of the curves.

5.3.2. Using only the data displayed in Fig. 5.2, which of these point processes are likely represented by: (i) a fractal-based point process, (ii) a fractal point process, (iii) a fractal renewal process, (iv) a fractal-rate point process?

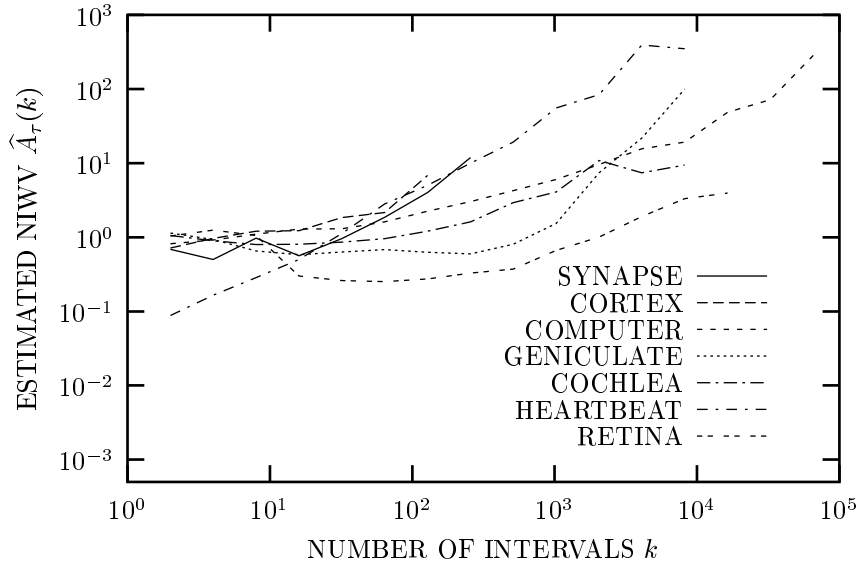


Fig. 5.8 Estimated normalized interval wavelet variance (NIWV), $\hat{A}_\tau(k)$ vs. number of intervals k , for the same seven point processes displayed in Fig. 5.2. We employed the Haar wavelet for these calculations. The curves increase roughly as straight lines, indicating an approximate power-law dependence on the number of intervals, with seven positive estimated power-law exponents $\hat{\alpha}_{A\tau}$.

5.3.3. Now, consider the curves displayed in Fig. 5.8 together with those shown in Fig. 5.2. Using the information provided by both measures, which of the point processes are likely represented by: (i) a fractal-based point process, (ii) a fractal point process, (iii) a fractal renewal process, (iv) a fractal-rate point process?

5.3.4. Can $\hat{A}_\tau(k)$ provide a good estimate of the fractal exponent?

5.3.5. Why is $k = 2$ the minimum number of intervals plotted for $\hat{A}_\tau(k)$?

5.4 Interevent-interval histograms for experimental point processes In Fig. 5.9, we present plots of the normalized interevent-interval histogram, $\hat{p}_\tau(\tau/\hat{E}[\tau])$ vs. normalized interevent interval $\tau/\hat{E}[\tau]$ [see Eq. (3.3)], for the seven experimental point processes considered earlier, presented on doubly logarithmic coordinates.

5.4.1. Based on the curves provided in Fig. 5.9, determine which of the underlying point processes can conceivably be represented by: (i) a fractal-based point process, (ii) a fractal point process, (iii) a fractal renewal process, (iv) a fractal-rate point process.

5.4.2. Now consider also the conclusions reached in the solutions of Probs. 5.2 and 5.3. Which of the point processes are likely represented by: (i) a fractal-based point process, (ii) a fractal point process, (iii) a fractal renewal process, (iv) a fractal-rate point process?

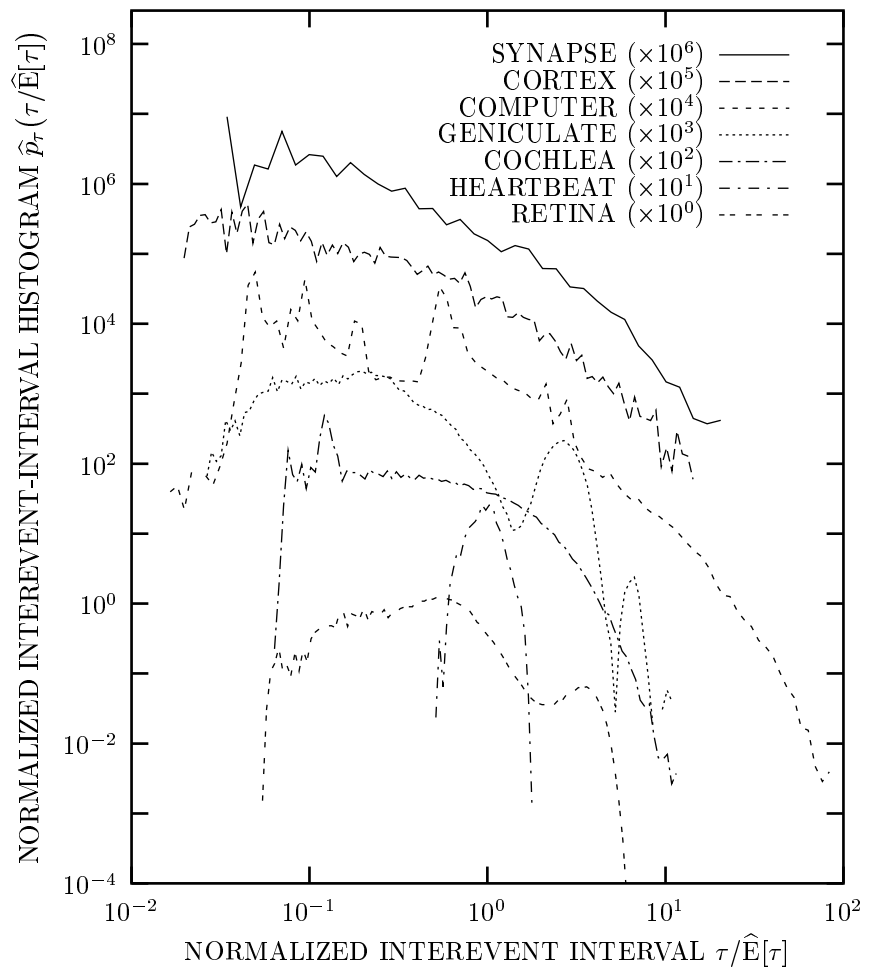


Fig. 5.9 Estimated normalized interevent-interval histogram, $\hat{p}_\tau(\tau/\hat{E}[\tau])$ vs. normalized interevent interval $\tau/\hat{E}[\tau]$, for the same seven point processes displayed in Figs. 5.1 and 5.2. We constructed these histograms by employing 100 geometrically spaced bins, from the smallest to the largest interevent interval, with the exception of SYNAPSE, for which we used 45 bins to improve the presentation. When no intervals fell into a particular bin, we eliminated it; bins that contained intervals but were flanked on either side by empty bins also do not appear. Little information is lost by making use of this procedure.

5.5 Generalized-dimension estimates for experimental point processes As the solutions to problems 5.2–5.4 show, the seven representative data sets discussed in this chapter clearly belong to the family of *fractal-based* point processes. Moreover, as we demonstrate in Sec. 11.5, the use of surrogate data sets (see Figs. 11.13 and

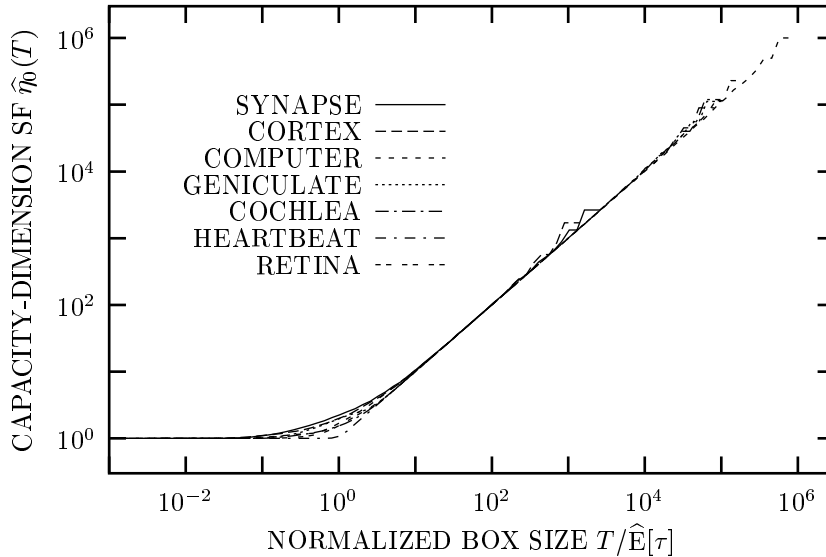


Fig. 5.10 Capacity-dimension scaling functions (SF) $\hat{\eta}_0(T)$, based on Eq. (3.74), for the same seven point processes displayed in Figs. 5.1 and 5.2. All curves resemble those for the nonfractal homogeneous Poisson point process shown in Fig. B.3. All of the data sets displayed here are described by *fractal-rate* point processes.

11.14) will lead us to conclude that none of the seven are *fractal renewal* point processes. However, to determine whether the larger class of *fractal* point processes describes any of these data (see Sec. 5.5.1), we examine the generalized dimensions D_q considered in Sec. 3.5.4.

To facilitate comparison across different values of q , we make use of a doubly logarithmic plot of the generalized-dimension scaling function $\eta_q(T)$ provided in Eq. (3.73). These sums yield parallel curves for nonfractal and monofractal data sets and are therefore easier to visualize than the sums provided in Eq. (3.72), which have slopes that vary with q . For comparisons among data sets, it is also convenient to normalize the counting time to the mean interevent interval $\hat{E}[\tau]$.

Figure 5.10 presents the capacity-dimension scaling function $\eta_0(T)$ for the seven canonical data sets considered earlier in this Chapter, calculated in accordance with Eq. (3.74).

5.5.1. Begin by simulating a homogeneous Poisson process (see Sec. 4.1), and a fractal renewal process with $\gamma = \frac{1}{2}$ and $B = \infty$ (see Sec. 4.2 and Ch. 7). For each process, generate 10^5 intervals, and normalize them by the estimated mean interval. Although this fractal renewal process has an infinite mean, the 10^5 intervals in the simulated realization will have a well-defined average value suitable for normalization (see Sec. 7.3). Display the capacity-dimension scaling function $\eta_0(T)$ vs. the normalized counting time $T/\hat{E}[\tau]$ on a doubly logarithmic plot. Include the theoret-

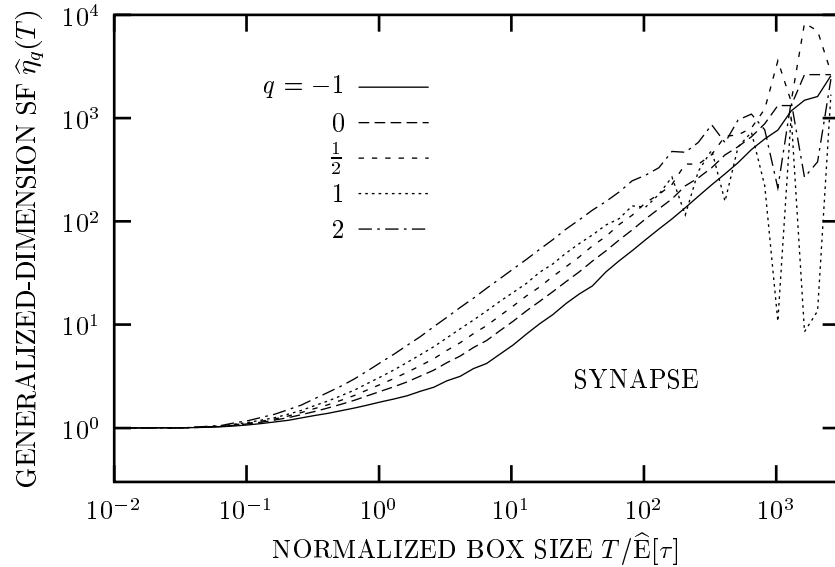


Fig. 5.11 Generalized-dimension scaling functions (SF) $\hat{\eta}_q(T)$ for various values of q , based on Eq. (3.73), for spontaneous vesicular exocytosis at a developing *Xenopus* neuromuscular junction (SYNAPSE) (Lowen et al., 1997b, cell 950315e1). A *fractal-rate* point process describes these data. Analogous curves for the action-potential sequence at a visual-system INTERNEURON appear in Fig. 11.18.

ical form for the homogeneous Poisson process considered in Prob. 4.3, as well as a curve proportional to $T^\gamma = \sqrt{T}$ for the fractal renewal process (see Sec. 7.2.5).

5.5.2. Compare the experimental capacity-dimension scaling functions displayed in Fig. 5.10 with those shown in Fig. B.3, focusing on the slopes of the curves at small and large values of the normalized time. What conclusions can you draw? Why is the sharpness of the transition region in the vicinity of $T = \hat{E}[\tau]$ different for the various curves?

5.5.3. Of all the data sets examined, Fig. 5.10 reveals that the capacity-dimension scaling function $\hat{\eta}_0(T)$ for the SYNAPSE data has the most gradual transition between the slopes of zero and unity. While this curve does not indicate the presence of fractal-point-process behavior, it does not exclude the possibility that similar curves using other values of q might. Generalized-dimension scaling functions for the SYNAPSE data with $q = -1, 0, \frac{1}{2}, 1,$ and 2 appear in Fig. 5.11. Can a fractal or multifractal point process describe these data? Why are the curves for the different values of q parallel but not coincident?

5.6 *Count autocorrelation function* Prove the last step before Eq. (5.13) in greater detail.

5.7 Cutoff relationship for unity fractal exponent Observe that the expressions for $\alpha < 1$ and $\alpha > 1$ in Eq. (5.48) are identical. Show that taking the limit $\alpha \rightarrow 1$ in either of these expressions yields the result provided for $\alpha = 1$.

5.8 Statistics for unity fractal exponent Starting with the spectrum provided in Eq. (5.46a), and assuming an abrupt low-frequency cutoff given by $f > 1/B$, prove the other relationships in Eq. (5.46). Consider the limit $kT/B \ll 1$. *Hint:* Prove them in the order b), c), e), and d).

5.9 Increasing coincidence rate Consider a coincidence rate that *increases* in a power-law fashion with delay time ($\alpha > 1$). As set forth in Eq. (5.44e), the functional form of such a coincidence rate would increase without bound for $\alpha > 1$. In an attempt to avoid this flaw, we introduce an exponential cutoff at a large time B :

$$G(t) = E[\mu] \delta(t) + E^2[\mu] \left[1 + \text{sgn}(t_G) (|t/t_G|)^{\alpha-1} e^{-|t|/B} \right]. \quad (5.50)$$

Again, $\text{sgn}(\cdot)$ denotes the sign of the argument.

Calculate the corresponding spectrum $S_N(f)$ and normalized variance $F(T)$ for $1 < \alpha < 3$, and show that one of these quantities must assume negative values for at least some times or frequencies. Since such behavior is inadmissible, what conclusions can you draw about the functional form of the coincidence rate given in Eq. (5.50)?

5.10 Long-time-scale statistics for negative fractal exponents Show that Eq. (5.17) indeed approaches Eq. (5.20) in the low-frequency limit $f \ll f_S$. Use the relationships provided in Chapter 3 to derive Eqs. (5.19) and (5.21) from Eq. (5.20).

5.11 Statistics for negative fractal exponents Use Eq. (5.15) (corresponding to $\alpha = -\frac{1}{2}$) to prove Eq. (5.17) for the normalized variance. Indicate how Eqs. (5.16) and (5.18) for the coincidence rate and normalized Haar-wavelet variance are obtained therefrom.

5.12 Rate-spectrum scaling-exponent limits for data with nonstationary rates Calculation of the normalized variance and normalized Haar-wavelet variance for data with a nonstationary rate often produces fractal exponents that attain the maximum allowed values of 1 and 3, respectively, as shown in Secs. 5.2.3 and 5.2.4. Determine the behavior of the rate-spectrum fractal exponent for data that exhibits a nonstationary rate.

5.13 Fractal behavior in nonstationary sets of points The validity of the relationships provided in Chapter 3, which are used throughout, generally requires stationarity. The Cantor set, described in Sec. 2.4.1, provides an example of a nonstationary set of points that highlights the limitations of these results for nonstationary processes (Lowen & Teich, 1995).

Consider a modification of the Cantor set construction procedure, in which we remove each closed interval from C_m and replace it with a single point event at its lower limit to yield a point process version thereof, $dN_m(t)$. The first three members

of this series become

$$\begin{aligned} dN_0(t) &= \delta(t) \\ dN_1(t) &= \delta(t) + \delta\left(t - \frac{2}{3}\right) \\ dN_2(t) &= \delta(t) + \delta\left(t - \frac{2}{9}\right) + \delta\left(t - \frac{2}{3}\right) + \delta\left(t - \frac{8}{9}\right), \end{aligned} \quad (5.51)$$

which follow from the rule

$$dN_{m+1}(t) = dN_m(t) \star [\delta(t) + \delta(t - 2/3^m)], \quad (5.52)$$

where \star denotes the convolution operation.

5.13.1. Show that the normalized variance⁹ for $dN_{m+1}(t)$ does indeed exhibit scaling behavior, reflecting the fractal characteristics of this set of points.

5.13.2. Now demonstrate that the spectrum does *not* reveal scaling behavior. Comment on the applicability of the central results of fractal-based point processes to nonstationary sets of points.

⁹ Since the collection of points under study originates via a deterministic process, it exhibits no randomness so that notions like variance and spectrum do not strictly apply. However, we treat the sets $dN_m(t)$ as if they were indeed random processes, and derive the statistical measures accordingly.